Analytical Quantum-Confinement Model for Short-Channel Gate-All-Around MOSFETs Under Subthreshold Region

Yu-Sheng Wu, *Student Member, IEEE*, and Pin Su, *Member, IEEE*

***Abstract*—This paper presents an analytical model for quantum-confinement effects in short-channel gate-all-around (GAA) MOSFETs under the subthreshold region. Our analytical model accurately predicts the impact of short-channel effects and doping concentration on the quantum-confinement effects. This scalable quantum-confinement model is crucial to the ultrascaled GAA MOSFET design.**

***Index Terms*—Gate-all-around (GAA), MOSFET, quantum effects, short-channel effect.**

I. Introduction

GATE-ALL-AROUND (GAA) MOSFET is an ideal structure to provide superior electrostatic behavior and is recognized as an important candidate for ultimate CMOS scaling [1]–[3]. As the channel thickness of GAA MOSFETs scales down, the quantum-confinement effects become significant. This 2-D confinement effect is often considered to be independent of the carrier flow direction (i.e., channel length direction). Thus, the quantum-confinement model for long-channel and undoped cylindrical GAA MOSFETs was proposed using the flat-well approximation [3], [4]. For short-channel devices, however, the center of the potential well is altered by the source/drain coupling due to the short-channel effect, and the flat-well approximation is no longer valid. An accurate quantum-confinement model considering the short-channel effects is crucial to GAA MOSFET design.

In this paper, an analytical solution of Schrödinger equation for short-channel GAA MOSFETs under the subthreshold region is proposed. The subthreshold behaviors represent the device electrostatic integrity that is important for ultrascaled device design. Aside from the lightly doped GAA MOSFETs, our analytical model can also be used for heavily doped devices.

This paper is organized as follows. In Section II, we demonstrate the method to derive the analytical solution of Schrödinger equation for short-channel GAA MOSFETs under the subthreshold region. In Section III, we verify our calculated eigenenergies and eigenfunctions with TCAD simulation. Some insights of quantum-confinement effects in GAA MOSFETs will be discussed. Finally, the conclusions will be drawn in Section IV.

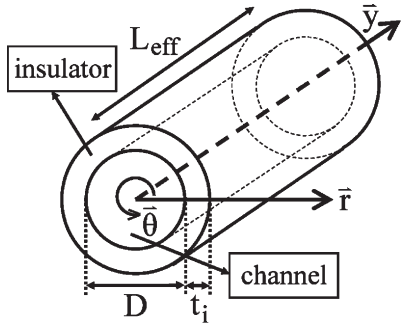

Fig. 1. Schematic sketch of the GAA structure investigated in this paper. The origin point $(r = 0, y = 0)$ is defined at the center of the channel/source junction.

II. Analytical Solution of Schrödinger Equation

The eigenenergy and eigenfunction of channel carriers are crucial to the quantum-confinement effect, and they can be determined by solving the Schrödinger equation. Fig. 1 shows a schematic sketch of the GAA MOSFET structure. The Schrödinger equation in the cylindrical coordinate is

$$-\frac{\hbar^2}{2m^*}\left(\frac{\partial^2}{\partial r^2}+\frac{1}{r}\frac{\partial}{\partial r}+\frac{1}{r^2}\frac{\partial^2}{\partial \theta^2}\right)\Psi(r,\theta)+E_C(r,\theta)\cdot\Psi(r,\theta) = E\cdot\Psi(r,\theta) \quad (1)$$

where E is the eigenenergy, $\Psi(r,\theta)$ is the corresponding wavefunction, $\hbar$ is the reduced Plank constant, and m^* is the effective mass of electron. In this paper, we consider the effective mass of the fourfold degenerate valleys as $2m_l \cdot m_t/(m_l + m_t)$ and that of the twofold degenerate valleys as m_t [5]–[8], with m_l and m_t being the longitudinal and transverse effective masses, respectively. It should be noted that an approximated isotropic effective mass is used in (1) to preserve the symmetric property in the cylindrical coordinate. This isotropic-mass approximation has also been employed by Jin *et al.* [5], [6] and Gnani *et al.* [7] in the studies of silicon nanowires and has been shown to yield reasonably accurate subband energy levels.

Manuscript received April 16, 2009; revised July 21, 2009. Current version published October 21, 2009. This work was supported in part by the National Science Council of Taiwan under Contract NSC 98-2221-E-009-178 and in part by the Ministry of Education in Taiwan under the ATU Program. The review of this paper was arranged by Editor C. McAndrew.

The authors are with the Department of Electronics Engineering, National Chiao Tung University, Hsinchu 30013, Taiwan (e-mail: pinsu@mail.nctu.edu.tw).

Color versions of one or more of the figures in this paper are available online at http://ieeexplore.ieee.org.

Digital Object Identifier 10.1109/TED.2009.2030714

The conduction band edge $E_C(r,\theta)$ in (1) can be obtained from the channel potential solution of Poisson's equation. In our previous work [9], we have derived the channel potential solution $\phi(r,y)$ for GAA MOSFETs in the subthreshold region

$$\phi(r,y) = \phi_1(r) + \phi_2(r,y) \tag{2a}$$

$$\phi_1(r) = Ar^2 + B \tag{2b}$$

$$\phi_2(r,y) = \sum_n \lfloor k_n \cdot \sinh(\lambda_n \cdot y) + k_n' \sinh\left(\lambda_n(L_{\text{eff}} - y)\right)\rfloor \cdot J_0(\lambda_n \cdot r) \tag{2c}$$

where L_{eff} is the channel length and $J_v(x)$ is the Bessel function of the first kind of order v. λ_n can be determined by

$$J_0\left(\lambda_n \frac{D}{2}\right) - \frac{\varepsilon_{\text{si}}}{C_i}\lambda_n J_1\left(\lambda_n \frac{D}{2}\right) = 0 \tag{3a}$$

$$C_i = \frac{2\varepsilon_i}{\left(D \cdot \ln(1 + \frac{2t_i}{D})\right)} \tag{3b}$$

where ε_{si} and ε_i are dielectric constants of the Si-channel and gate insulator, respectively. D and t_i are the channel diameter and thickness of gate insulator, respectively. Note that (3b) is the capacitance per unit length for an infinitely long cylindrical capacitor, which neglects the fringing effect of the field near the edges of the capacitor [10]. The coefficients A, B, k_n, and k_n' in (2a)–(2c) can be expressed as

$$A = -\frac{qN_a}{4\varepsilon_{\text{si}}} \tag{4a}$$

$$B = V_{\text{GS}} - V_{\text{fb}} + \frac{qN_a}{\varepsilon_{\text{si}}}\frac{D}{2}\left(\frac{D}{2} + 2\frac{\varepsilon_{\text{si}}}{C_i}\right) \tag{4b}$$

$$k_n = \frac{2}{\left[\left(\frac{C_i}{\lambda_n \varepsilon_{\text{si}}}\right)^2 + 1\right] \cdot J_0^2\left(\lambda_n \frac{D}{2}\right) \cdot \sinh\left(\lambda_n L_{\text{eff}}\right)} \cdot \left\{ -A \cdot \left[\frac{1}{\lambda_n}\left(\frac{D}{2}\right)^3 \cdot J_1\left(\lambda_n \frac{D}{2}\right) - 2\left(\frac{1}{\lambda_n}\right)^2\left(\frac{D}{2}\right)^2 \cdot J_2\left(\lambda_n \frac{D}{2}\right)\right] + (V_{\text{DS}} - \phi_{\text{ms}} - B)\frac{1}{\lambda_n}\frac{D}{2} \cdot J_1\left(\lambda_n \frac{D}{2}\right)\right\} \tag{4c}$$

$$k_n' = \frac{2}{\left[\left(\frac{C_i}{\lambda_n \varepsilon_{\text{si}}}\right)^2 + 1\right] \cdot J_0^2\left(\lambda_n \frac{D}{2}\right) \cdot \sinh\left(\lambda_n L_{\text{eff}}\right)} \cdot \left\{ -A\left[\frac{1}{\lambda_n}\left(\frac{D}{2}\right)^3 \cdot J_1\left(\lambda_n \frac{D}{2}\right) - 2\left(\frac{1}{\lambda_n}\right)\left(\frac{D}{2}\right)^2 \cdot J_2\left(\lambda_n \frac{D}{2}\right)\right] + (-\phi_{\text{ms}} - B)\frac{1}{\lambda_n}\frac{D}{2} \cdot J_1\left(\lambda_n \frac{D}{2}\right)\right\} \tag{4d}$$

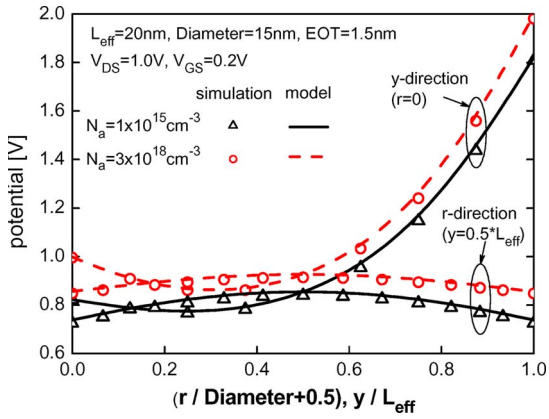

Fig. 2. Analytical potential distribution of GAA MOSFETs compared with TCAD simulation. A midgap workfunction of 4.5 eV is used.

where N_a is the channel doping. V_{GS} is the voltage bias of the gate terminal, and V_{fb} is the flatband voltage. V_{DS} is the voltage bias of the drain terminal, and ϕ_{ms} is the built-in potential of the source/drain to the channel. The verification of the channel potential solution with TCAD simulation is shown in Fig. 2.

To simplify the solution of the Schrödinger equation, the Bessel-function-based ϕ_2 is further reduced to the parabolic form, and E_C can be expressed as $E_C = \alpha \cdot r^2 + \beta$ with

$$\alpha = (-q) \cdot \left[A + \sum_n \left(-\frac{1}{4}\lambda_n^2\right) \cdot \left[k_n \cdot \sinh(\lambda_n \cdot y) + k_n' \cdot \sinh\left(\lambda_n(L_{\text{eff}} - y)\right)\right]\right] \tag{5a}$$

$$\beta = (-q) \cdot \left\{B + \sum_n \left[k_n \cdot \sinh(\lambda_n \cdot y) + k_n' \cdot \sinh\left(\lambda_n(L_{\text{eff}} - y)\right)\right] - \left[\frac{1}{2} \cdot \frac{E_g}{q} + \frac{1}{2}\frac{kT}{q} \cdot \ln\left(\frac{N_c}{N_v}\right)\right]\right\} \tag{5b}$$

where kT/q is the thermal voltage and E_g is the bandgap of Si channel. N_c and N_v are effective densities of states (DOSs) for conduction and valence bands, respectively.

By using the separation of variables technique, the solution of (1) can be expressed as $\Psi_{n,l}(r,\theta) = R_n(r) \cdot \exp(i \cdot l \cdot \theta)$ [11], with n and l being the principle quantum number and the angular quantum number, respectively. It should be noted that the angular quantum number l is restricted to integers $(0, \pm 1, \pm 2, \ldots)$ because of the periodicity of θ. Thus, $R_n(r)$ is the solution of

$$r^2 \cdot \frac{d^2R_n(r)}{dr^2} + r \cdot \frac{dR_n(r)}{dr} + \left\{\frac{2m^*r^2}{\hbar^2}\left[E_n - \left(\alpha \cdot r^2 + \beta\right)\right] - l^2\right\} \cdot R_n(r) = 0 \tag{6}$$

where $R_n(r)$ can be expressed as [12]

$$R_n(r) = \sum_{i=0}^{\infty} c_i \cdot r^{2i+l} \tag{7a}$$

with the coefficients c_i's being determined by the recurrence relationship

$$c_1 = -\frac{2m^*}{\hbar^2}\cdot\frac{(E_n-\beta)}{4\,(l+1)}\cdot c_0$$

$$c_i = -\frac{2m^*}{\hbar^2}\cdot\frac{(E_n-\beta)\cdot c_{i-1}-\alpha\cdot c_{i-2}}{4\cdot i^2+4\cdot i\cdot l},\quad i\geq 2. \tag{7b}$$

Generally, 20 terms in the summation of (7a) are needed to give sufficiently accurate results. It should be noted that, as $\alpha = 0$ (i.e., E_C is spatially constant), $R_n(r)$ will return to the form of Bessel function, which is the solution for long-channel and undoped GAA devices [3], [4]. The nth eigenenergy E_n can be determined by the boundary condition $R_n(r = D/2) = 0$. Thus, the eigenenergy and eigenfunction for short-channel GAA MOSFETs under the subthreshold region can be derived.

By using the calculated eigenenergies and eigenfunctions, we can calculate the electron density in the channel. The electron density can be expressed as

$$n(r,y) = N_{C,\mathrm{QM}}\cdot\exp\left(-\frac{E_C-E_F}{kT}\right) \tag{8a}$$

$$N_{C,\mathrm{QM}} = \sqrt{\frac{2kT}{\pi\hbar^2}}\cdot\sum_{i,n,l} g_i\cdot\sqrt{m^*_{di}}\cdot|\Psi_{i,n,l}(r,y)|^2 \cdot\exp\left(-\frac{E_{i,n,l}-E_C}{kT}\right) \tag{8b}$$

where g_i is the valley degeneracy and m^*_{di} is the DOS effective mass of valley i. In other words, the impact of quantized eigenenergies and eigenfunctions on the electron density is incorporated into the effective DOS for conduction band $(N_{C,\mathrm{QM}})$ [13].

III. Verification and Discussion

Fig. 3 shows the calculated quantized jth eigenenergy (E_j) and the square of jth eigenfunction $(|\Psi_j|^2)$ for lightly doped long-channel GAA devices, and the results are verified with TCAD simulation that numerically solves the self-consistent solution of 3-D Poisson and 2-D Schrödinger equations [8]. It can be seen that E_j and the difference between two distinct eigenenergies increase with decreasing channel diameter (D). Due to the cylindrical symmetry in the θ direction, E_2 and E_3 are degenerate because they correspond to the states of $l = 1$ and -1. Similarly, E_4 and E_5 are degenerate. The results in Fig. 3 can also be predicted by the quantum-confinement model using the flat-well approximation [3], [4]. For short-channel lightly doped GAA devices, however, the conduction band edge E_C is lowered by source/drain coupling and is bended from a flat well to a parabolic-like well (Fig. 4). Since E_C is not spatially constant for short-channel devices, we choose E_C at the channel center $(r = 0)$ as the reference energy. Fig. 4 shows that E_j's can be correctly predicted by our analytical solution considering the short-channel potential barrier. Fig. 5(a) shows that the lowest eigenenergy (E_1) increases as channel length decreases. This eigenenergy shift results from the bending of E_C due to the short-channel effect. Fig. 5(b)

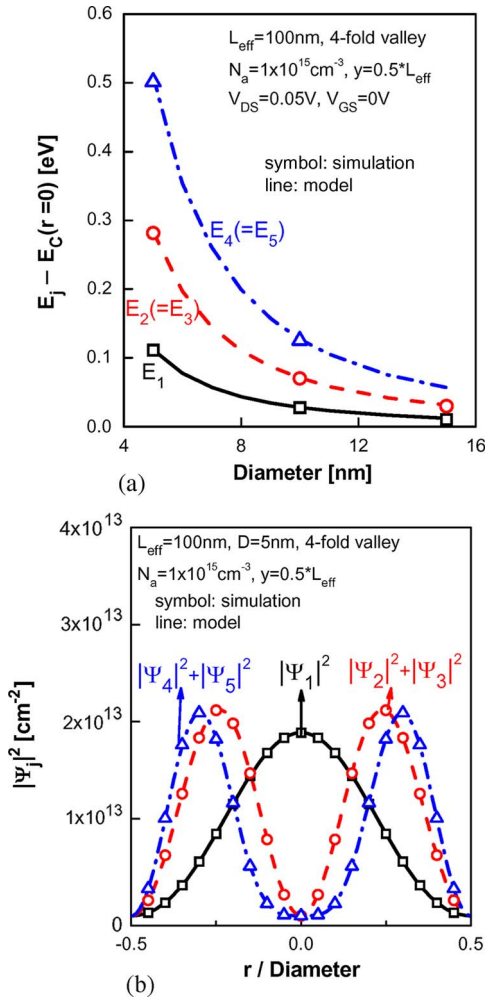

Fig. 3. (a) Quantized eigenenergies for long-channel lightly doped GAA devices. (b) Square of wavefunctions corresponding to the eigenenergies of GAA device with $D = 5$ nm in (a).

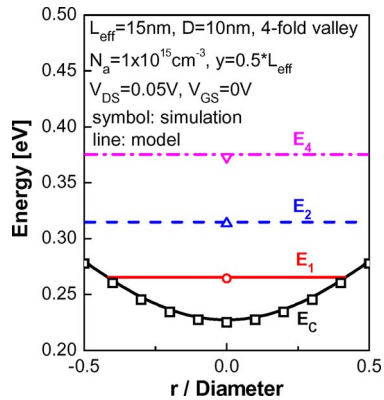

Fig. 4. Conduction band edge and quantized eigenenergies of a short-channel lightly doped GAA device.

shows that the square of lowest eigenfunction $(|\Psi_1|^2)$ for short-channel lightly doped device is more centralized to the channel center. This is because the E_C barrier at the channel center $(r = 0)$ is lower than that near the insulator/channel interface $(r = D/2)$ and the electron density becomes larger at $r = 0$. Fig. 6 shows that E_1 increases with V_{DS}. In other words, the

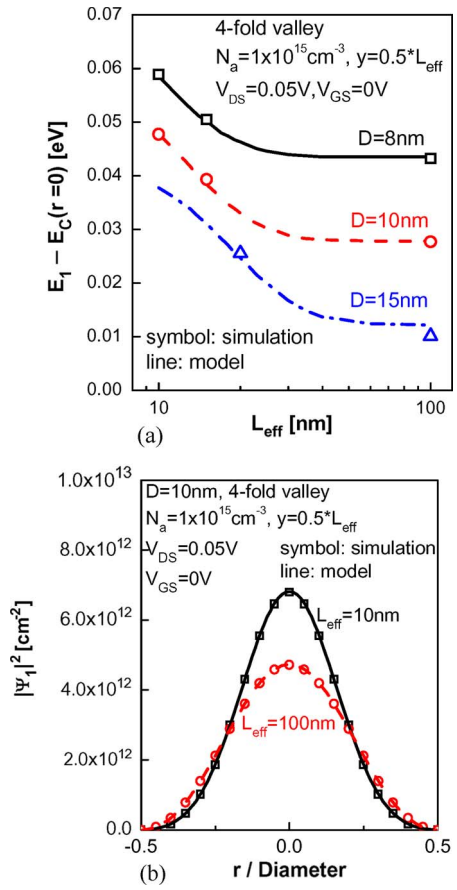

Fig. 5. (a) Channel length dependence of the first eigenenergy for lightly doped GAA devices with various channel diameters. (b) Comparison of the square of first eigenfunction for long-channel and short-channel GAA MOSFETs.

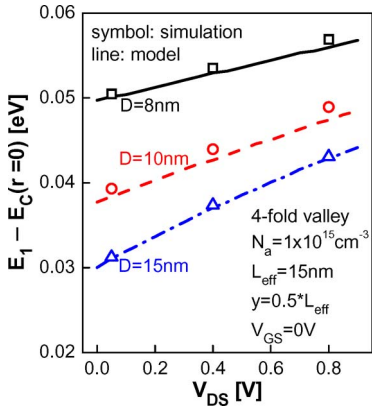

Fig. 6. Drain bias dependence of the first eigenenergy of short-channel lightly doped GAA devices with various channel diameters.

drain-induced-barrier-lowering (DIBL) increases the E_C bending and affects the quantum-confinement effects.

Our analytical model can also be used to assess the impact of quantum confinement on heavily doped GAA MOSFETs. Similar to the lightly doped short-channel devices, the E_C of heavily doped devices can be described by the parabolic form. In contrary to the upward bending of E_C in the lightly doped case, the E_C bends downward for heavily doped devices. Fig. 7 shows that the E_C for long-channel heavily doped GAA

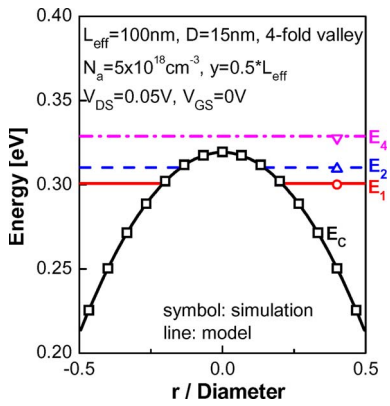

Fig. 7. Conduction band edge and quantized eigenenergies of a long-channel heavily doped GAA device.

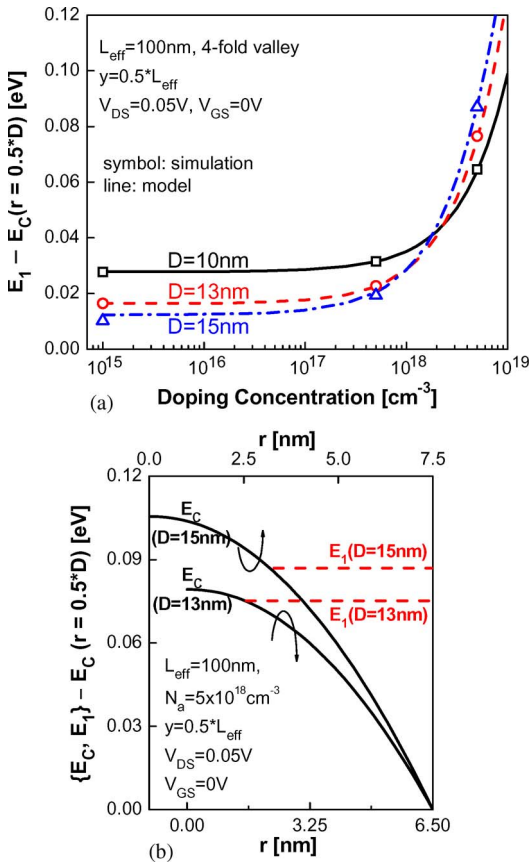

Fig. 8. (a) Impact of channel doping on the first eigenenergies of long-channel GAA devices with various channel diameters. The reference energy is defined at $E_C(r = 0.5 \cdot D)$. (b) First eigenenergies and conduction band edges of heavily doped GAA devices with $D = 13$ nm and $D = 15$ nm, respectively.

device shapes the potential well near the interface ($r = D/2$). Therefore, we choose the E_C at $r = D/2$ as the reference energy for long-channel GAA devices. Fig. 8(a) shows that the E_1 of long-channel GAA devices increases with channel doping. This is because as the channel doping increases, the surface electric field increases, and hence, the bending of E_C at the interface is increased. As a result, the E_1 increases due to the stronger electrical confinement. Moreover, it can be seen that, for heavily doped channels (e.g., 5×10^{18} cm^{-3}), E_1 increases with increasing channel diameter, which is

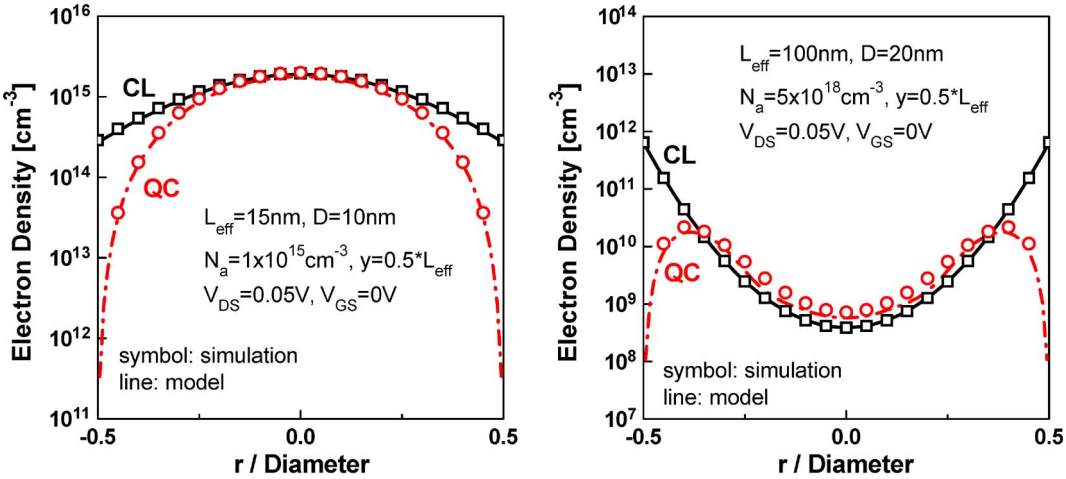

Fig. 9. Comparison of electron density distribution between classical (CL) model and quantum-confinement (QC) model. (a) Lightly doped short-channel GAA device. (b) Heavily doped long-channel GAA device.

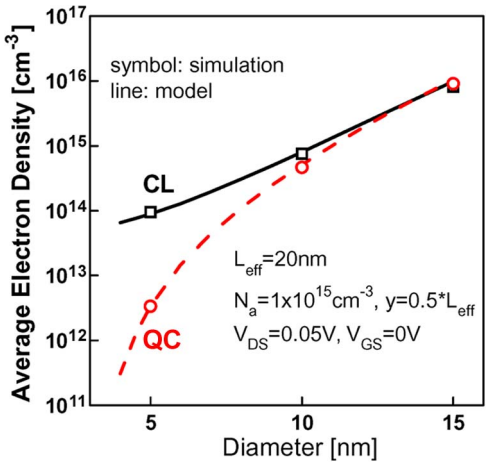

Fig. 10. Comparison of average electron density between CL model and QC model for lightly doped short-channel GAA MOSFETs with various channel diameters.

contrary to the lightly doped case (e.g., 1×10^{15} cm^{-3}). This is because for heavily doped devices, the electrical confinement becomes stronger with increasing channel diameter, as shown in Fig. 8(b).

Fig. 9 compares the electron density distributions calculated from the classical model [9] and the quantum-confinement model using (8). It can be seen from Fig. 9(a) that, for lightly doped short-channel GAA MOSFETs, the electron density near the interface ($r = D/2$) predicted by the quantum-confinement model is smaller than that predicted by the classical model. Fig. 9(b) shows that, for heavily doped long-channel GAA MOSFETs, the peak electron density predicted by the quantum-confinement model is away from the interface, while the classical model predicts the highest electron density at the interface. Furthermore, the average electron density can be calculated by $\int_0^{D/2} 2\pi \cdot r \cdot n(r,y)dr/A_{\rm ch}$, with $n(r,y)$ being the electron density derived from (8) and $A_{\rm ch}$ being the cross-sectional area of the channel. Fig. 10 compares the average electron densities at $y = 0.5L_{\rm eff}$ calculated from the classical model and the quantum-confinement model one for lightly doped short-channel devices. It can be seen that the discrepancy becomes larger with reducing channel diameter.

IV. Conclusion

We have proposed an analytical model for quantum-confinement effects in GAA MOSFETs under the subthreshold region. The Schrödinger equation is solved considering the bended potential well of parabolic form. Our analytical model accurately predicts the impact of short-channel effects on the eigenenergy and eigenfunction of GAA devices. This short-channel quantum-confinement model is crucial to the ultra-scaled GAA MOSFETs design.

References

[1] F. L. Yang, D. H. Lee, H. Y. Chen, C. Y. Chang, S. D. Liu, C. C. Huang, T. X. Chung, H. W. Chen, C. C. Huang, Y. H. Liu, C. C. Wu, C. C. Chen, S. C. Chen, Y. T. Chen, Y. H. Chen, C. J. Chen, B. W. Chan, P. F. Hsu, J. H. Shieh, H. J. Tao, Y. C. Yeo, Y. Li, J. W. Lee, P. Chen, M. S. Liang, and C. Hu, "5 nm-gate nanowire FinFET," in *VLSI Symp. Tech. Dig.*, Jun. 2004, pp. 196–197.

[2] N. Singh, A. Agarwal, L. K. Bera, T. Y. Liow, R. Yang, S. C. Rustagi, C. H. Tung, R. Kumar, G. Q. Lo, N. Balasubramanian, and D. L. Kwong, "High-performance fully depleted silicon nanowire (diameter $\leq$ 5 nm) gate-all-around CMOS devices," *IEEE Electron Device Lett.*, vol. 27, no. 5, pp. 383–386, May 2006.

[3] B. Yu, L. Wang, Y. Yuan, P. M. Asbeck, and Y. Taur, "Scaling of nanowire transistors," *IEEE Trans. Electron Devices*, vol. 55, no. 11, pp. 2846–2858, Nov. 2008.

[4] D. Jiménez, J. J. Sáenz, B. Iñíguez, J. Suñé, L. F. Marsal, and J. Pallarès, "Modeling of nanoscale gate-all-around MOSFETs," *IEEE Electron Device Lett.*, vol. 25, no. 5, pp. 314–316, May 2004.

[5] S. Jin, M. V. Fischetti, and T. W. Tang, "Theoretical study of carrier transport in silicon nanowire transistors based on the multisubband Boltzmann transport equation," *IEEE Trans. Electron Devices*, vol. 55, no. 11, pp. 2886–2897, Nov. 2008.

[6] S. Jin, M. V. Fischetti, and T. W. Tang, "Modeling of electron mobility in gated silicon nanowires at room temperature: Surface roughness scattering, dielectric screening, and band nonparabolicity," *J. Appl. Phys.*, vol. 102, no. 8, p. 083 715, Oct. 2007.

[7] E. Gnani, S. Reggiani, A. Gnudi, P. Parruccini, R. Colle, M. Rudan, and G. Baccarani, "Band-structure effects in ultrascaled silicon nanowires," *IEEE Trans. Electron Devices*, vol. 54, no. 9, pp. 2243–2254, Sep. 2007.

[8] *ATLAS User's Manual*, SILVACO, Santa Clara, CA, 2008.

[9] Y. S. Wu and P. Su, "Sensitivity of gate-all-around nanowire MOSFETs to process variations—A comparison with multigate MOSFETs," *IEEE Trans. Electron Devices*, vol. 55, no. 11, pp. 3042–3047, Nov. 2008.
[10] D. K. Cheng, *Field and Wave Electromagnetics*. Reading, MA: Addison-Wesley, 1992.
[11] J. H. Davies, *The Physics of Low-Dimensional Semiconductors*. Cambridge, U.K.: Cambridge Univ. Press, 1998.
[12] D. G. Zill and M. R. Cullen, *Differential Equations With Boundary Value Problems*, 5th ed. Pacific Grove, CA: Brooks/Cole, 2001.
[13] H. Ananthan and K. Roy, "A compact physical model for yield under gate length and body thickness variations in nanoscale double-gate CMOS," *IEEE Trans. Electron Devices*, vol. 53, no. 9, pp. 2151–2159, Sep. 2006.

Yu-Sheng Wu (S'09) was born in Tainan, Taiwan, in 1982. He received the B.S. and M.S. degrees in electronics engineering from the Department of Electronics Engineering, National Chiao Tung University, Hsinchu, Taiwan, in 2004 and 2006, respectively, where he is currently working toward the Ph.D. degree at the Institute of Electronics.

His current research interests include the design and modeling of advanced CMOS devices.

Pin Su (S'98–M'02) received the B.S. and M.S. degrees in electronics engineering from the National Chiao Tung University, Hsinchu, Taiwan, and the Ph.D. degree from the Department of Electrical Engineering and Computer Sciences, University of California, Berkeley.

From 1997 to 2003, he conducted his doctoral and postdoctoral research in silicon-on-insulator (SOI) devices at Berkeley. He was also one of the major contributors to the unified BSIMSOI model, the first industrial standard SOI MOSFET model for circuit design. Since August 2003, he has been with the Department of Electronics Engineering, National Chiao Tung University, where he is currently an Associate Professor. He is the author or coauthor of over 85 research papers in referred journals and international conference proceedings. His research interests include silicon-based nanoelectronics, modeling and design for advanced CMOS devices, and device/circuit interactions in ultrascaled CMOS.